

Air-bridge and vertical CNT switches for high performance switching applications

A. B. Kaul, E. W. Wong, L. Epp, M. J. Bronikowski, and B. D. Hunt

ABSTRACT

Carbon nanotubes are attractive for switching applications since electrostatically-actuated CNT switches have low actuation voltages and power requirements, while allowing GHz switching speeds that stem from the inherently high elastic modulus and low mass of the CNT. Our first NEM structure, the air-bridge switch, consists of suspended single-walled nanotubes (SWNTs) that lie above a sputtered Nb base electrode, where contact to the CNTs is made using evaporated Au/Ti. Electrical measurements of these air-bridge devices show well-defined ON and OFF states as a dc bias of a few volts is applied between the CNT and the Nb-base electrode. The CNT air-bridge switches were measured to have switching times down to a few nanoseconds. Our second NEM structure, the vertical CNT switch, consists of nanotubes grown perpendicular to the substrate. Vertical multi-walled nanotubes (MWNTs) are grown directly on a heavily doped Si substrate, from 200 – 300 nm wide, $\sim 1 \mu\text{m}$ deep nano-pockets, with Nb metal electrodes to result in the formation of a vertical single-pole-double-throw switch architecture.

INTRODUCTION

Carbon nanotubes (CNTs) have remarkable mechanical and electrical properties which makes them excellent candidates for the design of nanoelectromechanical systems (NEMS). Nanotube based NEMS have already been demonstrated in applications ranging from nanotweezers,¹ memory devices,² supersensitive sensors³ and tunable oscillators.⁴ Nanorelays^{5,6} are another promising application of nanotubes that offer the potential for high performance switching, with high speed operation at low actuation voltages and power.

Although theoretical studies on CNT switches have been reported,^{5,7} results from fabricated devices that characterize nanoscale electromechanical switching have been limited. To date, switching in both SWNTs² and MWNTs^{8,9,10} has been with deposited tubes. Here we demonstrate switching results for SWNT air-bridge devices, where the tubes are grown on-chip with patterned catalysts using materials that are compatible with the high temperature CVD synthesis of SWNTs. We also present process development results for vertical MWNTs formed into single-pole-double-throw switch configurations that can enable high density 3-D integration.

EXPERIMENT

A schematic of our first NEM structure, the air-bridge device, is shown in Fig. 1a. The fabrication details of this structure have been described elsewhere.¹¹ A schematic of the vertical CNT switch is shown in Fig. 1b, where the MWNTs are grown directly on a conducting Si substrate to form a ground contact to the CNT. The process development results for the vertical switch are discussed in more detail in the discussion section.

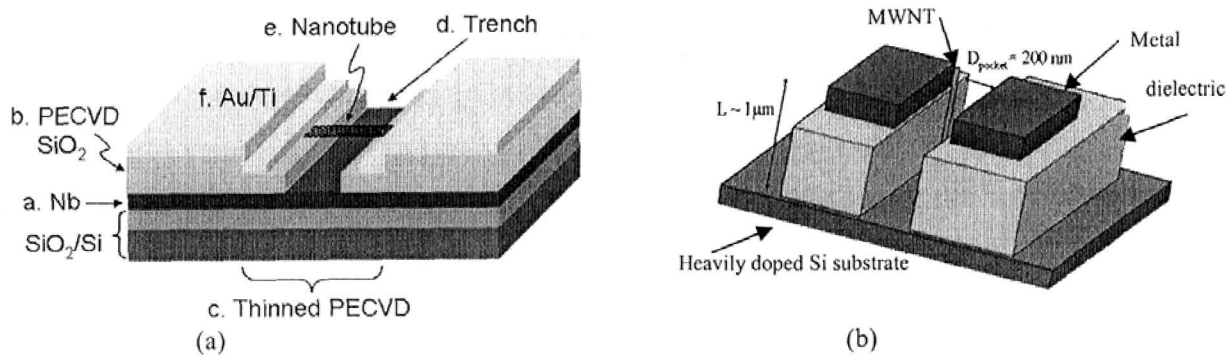


Figure 1. (a) Air-bridge CNT switch schematic. (b) Vertical CNT switch schematic.

DISCUSSION

Air-bridge CNT switch

An SEM micrograph of a finished air-bridge device is shown in Fig. 2a, where the underlying Nb pull electrode in the nanotrench is contacted by the Au/Ti electrodes labeled “pull”. Also shown are the source and drain electrodes which contact the CNT that bridges the trench. The high magnification SEM image of Fig. 2b depicts a nanotube crossing the trench. The conductance between the source and drain electrodes typically ranged in value from tens of $k\Omega$ to tens of $M\Omega$, where the presence of multiple tubes can also contribute to the differences in resistance.

The actuation voltages were measured by applying a dc voltage between the source and pull electrodes. As transient charge develops on the tube with increasing bias voltage, the resulting electrostatic force is sufficient to overcome the elastostatic force and deflects the suspended tube down toward the pull electrode. The current was measured as a function of the dc bias voltage between the source and pull electrodes. Shown in Fig. 3a is an I-V characteristic for the device illustrated in Fig. 2b. For voltages up to 2.0 V, the currents are very low, a few pA. Then from ~ 3.5 V, the current begins to rise rapidly to ~ 250 nA at ~ 4.5 V. This switching between the low- and high-current states represents more than a ~ 4 order of magnitude increase, implying well-defined OFF and ON states, respectively. The currents measured are believed to originate from a tunneling mechanism; as the tube deflects closer to the bottom electrode with increasing bias voltage, the magnitude of the tunnel current increases exponentially. In the rapidly rising current regime, the data is increasingly noisy, reflecting the stochastic nature of the tunneling mechanism.

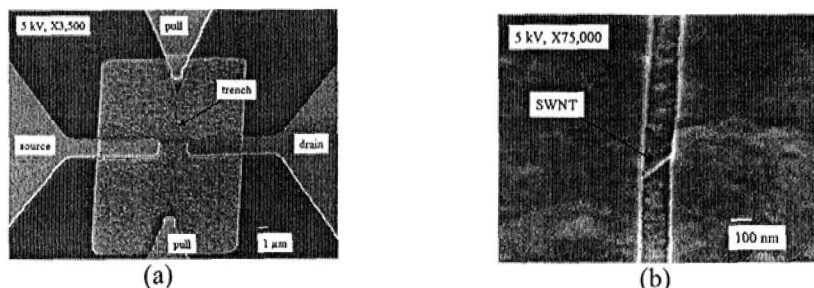


Figure 2. (a) SEM image of device. (b) High magnification SEM image showing a SWNT bridging the trench.

Hysteresis between the increasing and decreasing bias voltage paths was also evident, and arises from the interaction of the tube with surface van der Waals forces. Lateral leakage currents within the dielectric were extremely small, ~ 10 pA at ± 5 V, as indicated by currents in the absence of tubes. The rapidly rising current regime was found to arise in both the forward-biased (pull electrode grounded) and reverse-biased (pull electrode positive) cases, so this switching behavior is polarity independent, as would be expected for electrostatic actuation, and rules out field emission as a likely mechanism at these voltages.

The I-V characteristic in Fig. 3b is a representative example of a device in which stiction was observed. In this case, the current rises rapidly at 2.5 V and saturates at the instrumentation compliance which was set to ~ 20 μ A. On the decreasing-voltage path, an ohmic resistance was observed, which was typically in the range of a few k Ω to hundreds of k Ω . The ohmic behavior persisted upon subsequent cycling and the device appeared stuck. Dujardin¹⁰ *et al.* have noted that a decanethiol self-assembled monolayer (SAM) coating over the Au electrode that the CNT contacts sufficiently prevents stiction in their devices.

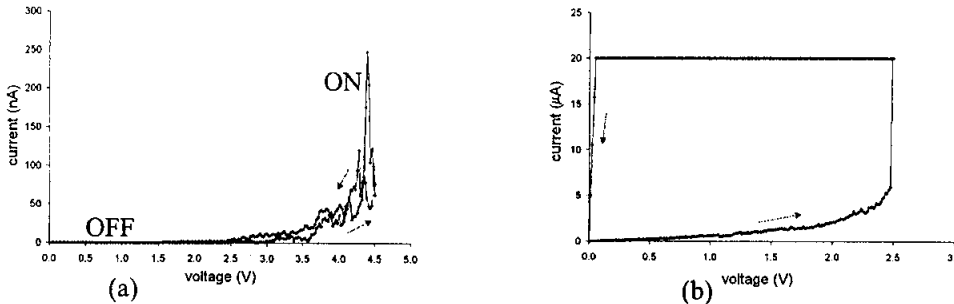


Figure 3. (a) I-V characteristic showing switching in a device at ~ 4.4 V. (b) An example of stiction observed in a device.

We have also performed switch speed measurements on our CNT air bridge devices. The measurement set-up is shown in Fig. 4a. The voltage applied by the pulse generator was incrementally increased by 200 mV intervals. Up to 4.8 V, no output pulse was detected. Then at ~ 5 V, the output voltage rapidly increased as shown in Fig. 4b (“switch output” waveform). The “calibration output” waveform refers to the case where the device was removed and the probes were placed on a metal strip on-chip to measure the intrinsic delay associated with the instrumentation, such as that arising from cable lengths, stray capacitances and inductances both on- and off-chip. The difference in time required to reach the maximum voltage between the two waveforms was determined to be ~ 2.8 ns, as indicated in Fig. 4b, yielding an upper bound of the intrinsic switching speed of the CNT switch. The oscillations in the calibration and switch waveforms likely arise from resonances associated with the lead-line inductances and the capacitances from the instrumentation; we do not have sufficient information available to calculate the nature of the damping mechanisms involved in these cases.

Compared to state-of-the-art MEMS devices, the switching times of our CNT switches are several orders of magnitude smaller. Peroulis¹² *et al.* reported total switching time for Si MEMS devices to be 52 μ s, for which the response time alone was ~ 30 μ s. The ultra-low mass, exceptionally high spring constant and extremely low capacitance of the CNT, all contribute to the small response and rise times in the CNT switch, which lead to the extremely small total switching times, as observed. The fastest MEMS switch was developed at MIT Lincoln Labs and is reported to have a switching time of 1 μ s; this was realized by decreasing device dimensions,

but there is a concomitant increase in the voltage, with 60-70 V needed for actuation.¹³ These voltages are difficult to obtain in applications where low-voltage power supplies are used, such as hand-held mobile phones and other wireless applications, as well as automotive vehicles. The CNT air bridge switch has the unique advantage of low actuation voltage < 5 V, while enabling nanosecond switching times.

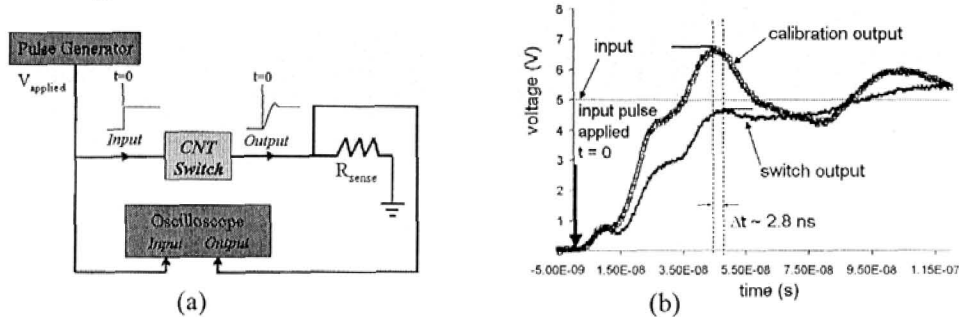


Figure 4. (a) Switching speed measurement set-up. (b) Switching observed in a device as indicated by the “switch output” waveform.

Vertical CNT switch

We have also developed a process for forming vertical CNT switches. The process used to form the devices is shown in Fig. 5, which requires nanotubes to grow from 200 – 300 nm wide, ~ 1 μm deep nanopockets. The MWNT growth is done directly on a heavily doped (3 $\text{m}\Omega\text{cm}$) conducting Si substrate thus forming a means to electrically contact the CNT, with the use of an Al interlayer between the Fe-catalyst.

CNT growth experiments from deep SiO_2 pockets were performed in order to form 1-2 μm long MWNTs. These tubes were grown at 575 C, 200 Torr ethylene for 2 minutes, resulting in growth rates of ~ 0.75 $\mu\text{m}/\text{min}$; an SEM image of typical CNTs emerging from the holes is shown in Fig. 6a. Most of the CNTs protrude out of the holes by 100 – 1000 nm. We have experimented with grazing angle ion milling to “trim” these CNTs. Ion milling was done at 10 degrees, 350 V for 15 minutes, and the SEM image in Fig. 6b shows the CNTs have indeed been “trimmed” as a result of the ion milling.

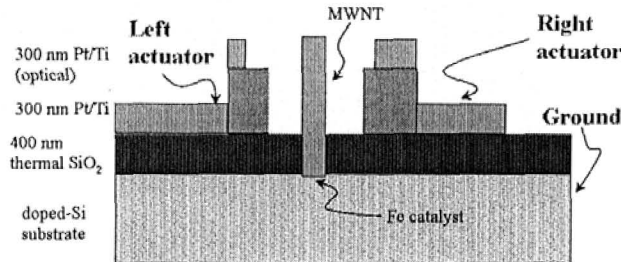


Figure 5. Process for vertical MWNT switch.

To form the deep, nanometer-sized SiO_2 pockets, we transferred the e-beam defined ZEP resist pattern into an Al hard mask material. Without a hard mask material it is difficult to etch far into the SiO_2 while still retaining a sufficient amount of e-beam resist. With the exceptionally high etch rates of metals and dielectrics obtained in inductively coupled plasma etchers (ICP), we have determined etch rates of Al to be ~ 300 nm/min using a Chlorine ICP etcher; a 100 nm thick Al mask layer can be etched in less than in 20 seconds. While most of the

ZEP is also etched in this process, there is still a small amount present that allows the e-beam pattern to be transferred into the Al layer. Shown in Fig. 6c is an SEM image of 300 nm wide pockets that have been transferred successfully from the ZEP into the Al mask material using 30 sccm of BCl_3 , 15 sccm of Cl_2 , 400 W ICP power and 30 W of bias power at a pressure of 5 mTorr.

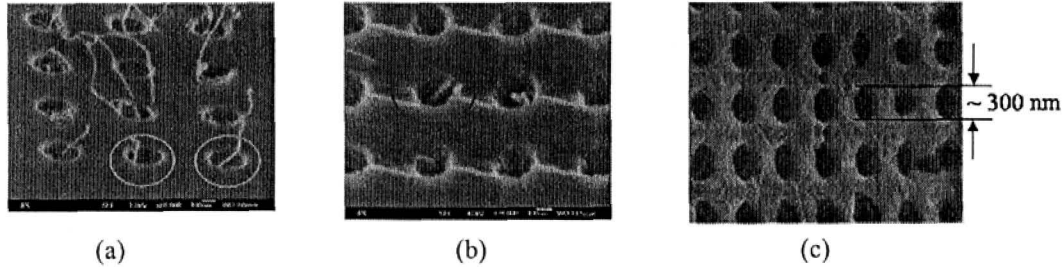


Figure 6. (a) MWNT growth from nano-pockets. (b) Grazing angle ion milling used to trim the CNT. (c) Nano-pockets formed using an Al hard mask material.

After forming the deep nanopockets with the Al hard mask, the 2.5 nm Fe catalyst and 3 nm Al interlayer were deposited using e-beam evaporation and lifted-off with the use of TMAH to remove the Al. For the metal electrodes, we experimented with evaporated Pt and Ti, as well as sputtered Nb that was deposited at near zero compressive stresses by tuning the Ar pressure during growth. The Ti electrodes however, were found to be attacked by the hydrogen during CNT growth due to the formation of volatile metal hydride. By reducing the exposure to hydrogen during the MWNT growth annealing step, this etching behavior was minimized.

Shown in Fig. 7a is a low magnification SEM image of a completed vertical CNT switch. The layout of the active region is shown in Fig. 7b and is compared to the high magnification SEM image in Fig. 7c., where Nb was used as the electrode material. These images were taken just prior to CNT growth, which is the last step in the process. Note that due to issues with e-beam alignment, the electrodes were offset to the right, which can be corrected in any future work.

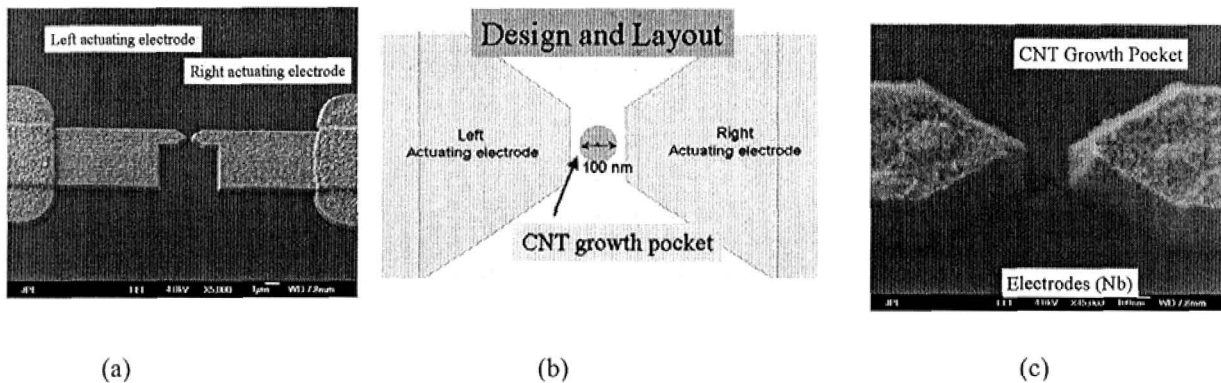


Figure 7. (a) SEM image of a completed vertical MWNT switch. (b) Layout and comparison to (c) fabricated device.

Shown in Fig. 8a and (b) are the devices after CNT growth. From these images it should be clear that the CNTs are indeed present, despite the fact that the Fe/Al catalyst was deposited early in the process, and survived the many process steps prior to MWNT growth. JPL has developed a vertical MWNT switch process, where the tubes have been demonstrated to grow

from deep within nanopockets on a conducting heavily doped Si-substrates with integrated Pt/Ti or Nb electrodes.

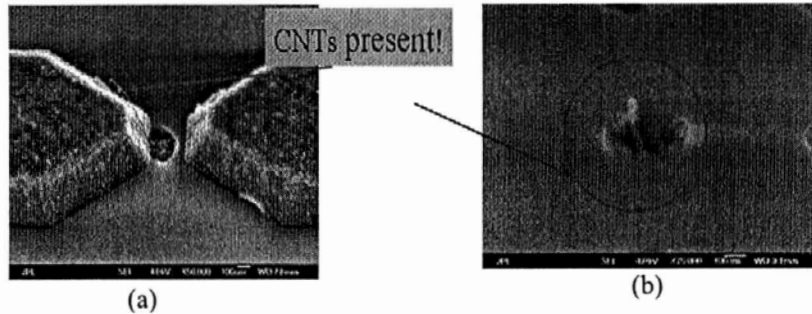


Figure 8. (a) Vertical MWNT switch devices showing the presence of CNTs. (b) CNTs are also present in the array patterns.

CONCLUSIONS

In summary, switching was demonstrated in air-bridge devices, with pull voltages of a few volts and switching times of a few nanoseconds. A vertical CNT switch process was also developed at JPL and described here. In conclusion, CNT based NEM switches can be enabling elements for communication networks and memory applications where ultra-miniaturized, light weight components that operate at low voltage, low power and high speed are required.

ACKNOWLEDGMENTS

We thank Richard E. Muller for e-beam patterning and Dr. Harish Manohara and Dr. Martin I. Herman for useful discussions. This research was carried out at the Jet Propulsion Laboratory, California Institute of Technology, under a contract with the National Aeronautics and Space Administration.

REFERENCES

- ¹ P. Kim and C. M. Lieber, *Science* **286**, 2148 (1999).
- ² T. Rueckes, K. Kim, E. Joselevich, G. Y. Tseng, C. L. Cheung, and C. M. Lieber, *Science* **289**, 94 (2000).
- ³ P. G. Collins, K. B. Bradley, M. Ishigamo, and A. Zettl, *Science* **287**, 120 (2000).
- ⁴ V. Sazonova, Y. Yaish, H. Ustunel, D. Roundy, T. A. Arias, and P. L. McEuen, *Nature* **431**, 284 (2004).
- ⁵ M. Dequesnes, S. V. Rotkin and N. R. Aluru, *Nanotech.* **13**, 120 (2002).
- ⁶ B. M. Segal, D. K. Block, R. Thomas, Electromechanical memory array using nanotubes ribbons and method for making same, US Patent 6,919,592, 2004.
- ⁷ J. M. Kinaret, T. Nord, and S. Viefers, *Appl. Phys. Lett.*, **82**, 1287 (2003).
- ⁸ S. W. Lee, D. S. Lee, R. E. Morjan, S. H. Jhang, M. Sveningsson, O. A. Nerushev, Y. W. Park, and E. E. B. Campbell, *Nano. Lett.* **4**, 2027 (2004).

⁹ S. N. Cha, J. E. Jang, Y. Choi, and G. A. J. Amaratunga, D. J. Kang, D. J. Hasko, J. E. Jung and J. M. Kim, Appl. Phys. Lett. **86**, 083105-1 (2005).

¹⁰ E. Dujardin, V. Derycke, M. F. Goffman, R. Lefevre, and J. P. Bourgoin, Appl. Phys. Lett. **87**, 193107-1 (2005).

¹¹ A. B. Kaul, E. W. Wong, L. Epp, and B. D. Hunt, accepted, to appear in Nano Letters

¹² D. Peroulis, S. P. Pacheco, K. Sarabandi, L. P. B. Katehi, IEEE Trans. on Microwave Theory and Tech. **51**, 259 (2003).

¹³ S. Duffy, et al., IEEE Microwave Wireless Comp. Lett. **11**, 106 (2001).